Observing Application

Date:	Aug 02, 2021
Proposal ID:	VLA/22A-179
Legacy ID:	AA529
PI:	Sean Andrews
Type:	Regular
Category:	Star Formation
Total time:	46.75

Detailed Microwave Spectra of Protoplanetary Dust Disks

Abstract:

We propose a pilot study that collects and analyzes sensitive, contemporaneous (within ~1 hour), and densely-sampled (1-2 GHz spectral resolution) measurements of the ~5-50 GHz continuum spectra emitted by nearby young protoplanetary disk systems. This first-of-its-kind systematic study of the detailed microwave spectra of disk targets will help us to constrain key global properties of the dust disks (e.g., mass, grain size distribution) based on their 20-50 GHz thermal dust continuum emission, with minimal contamination from the high optical depths than can plague measurements at >100 GHz. Moreover, we can characterize the properties of additional radio continuum emission mechanisms, without confusion from variability, to help better understand the links between accretion, outflow, and stellar activity during the epoch of planet formation.

Authors:

Name	Institution	Email	Status
Andrews, Sean	Center for Astrophysics | Harvard & Smithsonian	sandrews@cfa.harvard.edu	
Wilner, David	Center for Astrophysics | Harvard & Smithsonian	dwilner@cfa.harvard.edu	
Chandler, Claire	National Radio Astronomy Observatory	cchandle@nrao.edu	
Long, Feng	Center for Astrophysics | Harvard & Smithsonian	feng.long@cfa.harvard.edu	
Macias, Enrique	Joint ALMA Observatory	enrique.macias@alma.cl	
Carrasco-Gonzalez, Carlos	MÃ©xico, Universidad Nacional AutÃ³noma de	c.carrasco@irya.unam.mx	

Principal Investigator:	Sean Andrews
Contact:	Sean Andrews
Telephone:	617-496-7645
Email:	sandrews@cfa.harvard.edu

Related Proposals:

Joint:

Not a Joint Proposal.

Observing type(s):

Continuum

VLA Resources

Name	Conf.	Frontend & Backend	Setup
Q-phot	D	Q Band 0.7 cm 40000 - 50000 MHz General and Shared Risk Observing - Wideband	Basebands: 4 x 2 GHz(3-bit) Baseband centers (GHz): 41, 43, 45, 47 Total bandwidth (GHz): 8.0 Polarization products: Full Dump time (s): 3.0 Data rate: 15.8 MB/s, 56.9 GB/h
Ka-phot	D	Ka Band 0.9 cm 26500 - 40000 MHz General and Shared Risk Observing - Wideband	Basebands: 4 x 2 GHz(3-bit) Baseband centers (GHz): 30, 32, 34, 36 Total bandwidth (GHz): 8.0 Polarization products: Full Dump time (s): 3.0 Data rate: 15.8 MB/s, 56.9 GB/h
K-phot	D	K Band 1.3 cm 18000 - 26500 MHz General and Shared Risk Observing - Wideband	Basebands: 4 x 2 GHz(3-bit) Baseband centers (GHz): 19, 21, 23, 25 Total bandwidth (GHz): 8.0 Polarization products: Full Dump time (s): 3.0 Data rate: 15.8 MB/s, 56.9 GB/h
Ku-phot	D	Ku Band 2 cm 12000 - 18000 MHz General and Shared Risk Observing - Wideband	Basebands: 3 x 2 GHz(3-bit) Baseband centers (GHz): 13, 15, 17 Total bandwidth (GHz): 6.0 Polarization products: Full Dump time (s): 3.0 Data rate: 11.8 MB/s, 42.6 GB/h
X-phot	D	X Band 3.6 cm 8000 - 12000 MHz General and Shared Risk Observing - Wideband	Basebands: 2 x 2 GHz(3-bit) Baseband centers (GHz): 9, 11 Total bandwidth (GHz): 4.0 Polarization products: Full Dump time (s): 3.0 Data rate: 7.9 MB/s, 28.4 GB/h
C-phot	D	C Band 6 cm 4000-8000 MHz General and Shared Risk Observing - Wideband	Basebands: 2 x 2 GHz(3-bit) Baseband centers (GHz): 5, 7 Total bandwidth (GHz): 4.0 Polarization products: Full Dump time (s): 5.0 Data rate: 4.7 MB/s, 17.1 GB/h

Sources

Name	Position		Velocity		Group
AATau	**Coordinate system**	Equatorial	**Convention**	Radio	AA Tau
	Equinox	J2000			
	Right Ascension	04:34:55.42	**Ref. frame**	LSRK	
		00:00:00.0			
	Declination	+24:28:52.8	**Velocity**	0.00	
		00:00:00.0			
	Calibrator	No			

Name	Position		Velocity		Group
ABAur	Coordinate system	Equatorial	Convention	Radio	AB Aur
	Equinox	J2000			
	Right Ascension	04:55:45.70	Ref. frame	LSRK	
		00:00:00.0			
	Declination	+30:32:56.0	Velocity	0.00	
		00:00:00.0			
	Calibrator	No			
CITau	Coordinate system	Equatorial	Convention	Radio	CI Tau
	Equinox	J2000			
	Right Ascension	04:33:52.00	Ref. frame	LSRK	
		00:00:00.0			
	Declination	+22:50:30.0	Velocity	0.00	
		00:00:00.0			
	Calibrator	No			
CWTau	Coordinate system	Equatorial	Convention	Radio	CW Tau
	Equinox	J2000			
	Right Ascension	04:14:17.00	Ref. frame	LSRK	
		00:00:00.0			
	Declination	+28:10:57.6	Velocity	0.00	
		00:00:00.0			
	Calibrator	No			
DLTau	Coordinate system	Equatorial	Convention	Radio	DL Tau
	Equinox	J2000			
	Right Ascension	04:33:39.07	Ref. frame	LSRK	
		00:00:00.0			
	Declination	+25:20:38.0	Velocity	0.00	
		00:00:00.0			
	Calibrator	No			
DMTau	Coordinate system	Equatorial	Convention	Radio	DM Tau
	Equinox	J2000			
	Right Ascension	04:33:48.73	Ref. frame	LSRK	
		00:00:00.0			
	Declination	+18:10:09.8	Velocity	0.00	
		00:00:00.0			
	Calibrator	No			
DNTau	Coordinate system	Equatorial	Convention	Radio	DN Tau
	Equinox	J2000			
	Right Ascension	04:35:27.37	Ref. frame	LSRK	
		00:00:00.0			
	Declination	+24:14:58.7	Velocity	0.00	
		00:00:00.0			
	Calibrator	No			

Name	Position		Velocity		Group
DOTau	Coordinate system	Equatorial	Convention	Radio	DO Tau
	Equinox	J2000			
	Right Ascension	04:38:28.57	Ref. frame	LSRK	
		00:00:00.0			
	Declination	+26:10:49.4	Velocity	0.00	
		00:00:00.0			
	Calibrator	No			
DRTau	Coordinate system	Equatorial	Convention	Radio	DR Tau
	Equinox	J2000			
	Right Ascension	04:47:05.48	Ref. frame	LSRK	
		00:00:00.0			
	Declination	+16:58:42.1	Velocity	0.00	
		00:00:00.0			
	Calibrator	No			
FTTau	Coordinate system	Equatorial	Convention	Radio	FT Tau
	Equinox	J2000			
	Right Ascension	04:23:39.20	Ref. frame	LSRK	
		00:00:00.0			
	Declination	+24:56:14.2	Velocity	0.00	
		00:00:00.0			
	Calibrator	No			
GOTau	Coordinate system	Equatorial	Convention	Radio	GO Tau
	Equinox	J2000			
	Right Ascension	04:43:03.07	Ref. frame	LSRK	
		00:00:00.0			
	Declination	+25:20:18.6	Velocity	0.00	
		00:00:00.0			
	Calibrator	No			
Haro6-13	Coordinate system	Equatorial	Convention	Radio	Haro 6-13
	Equinox	J2000			
	Right Ascension	04:32:15.41	Ref. frame	LSRK	
		00:00:00.0			
	Declination	+24:28:59.5	Velocity	15.500	
		00:00:00.0			
	Calibrator	No			
IQTau	Coordinate system	Equatorial	Convention	Radio	IQ Tau
	Equinox	J2000			
	Right Ascension	04:29:51.55	Ref. frame	LSRK	
		00:00:00.0			
	Declination	+26:06:44.7	Velocity	0.00	
		00:00:00.0			
	Calibrator	No			

Name	Position		Velocity		Group
LkCa15	Coordinate system	Equatorial	Convention	Radio	LkCa 15
	Equinox	J2000			
	Right Ascension	04:39:17.79	Ref. frame	LSRK	
		00:00:00.0			
	Declination	+22:21:03.3	Velocity	17.650	
		00:00:00.0			
	Calibrator	No			
MWC480	Coordinate system	Equatorial	Convention	Radio	MWC 480
	Equinox	J2000			
	Right Ascension	04:58:46.26	Ref. frame	LSRK	
		00:00:00.0			
	Declination	+29:50:36.9	Velocity	0.00	
		00:00:00.0			
	Calibrator	No			
GMAur	Coordinate system	Equatorial	Convention	Radio	GM Aur
	Equinox	J2000			
	Right Ascension	04:55:10.97	Ref. frame	LSRK	
		00:00:00.0			
	Declination	+30:21:59.0	Velocity	0.00	
		00:00:00.0			
	Calibrator	No			
RYTau	Coordinate system	Equatorial	Convention	Radio	RY Tau
	Equinox	J2000			
	Right Ascension	04:21:56.74	Ref. frame	LSRK	
		00:00:00.0			
	Declination	+28:26:33.8	Velocity	0.00	
		00:00:00.0			
	Calibrator	No			

Sessions:

Name	Session time (hours)	Repeat	Separation	LST minimum	LST maximum	Elevation minimum
CW Tau phot	2.75	1	0 day	00:19:03	08:09:31	40
RY Tau phot	2.75	1	0 day	00:26:14	08:17:40	40
FT Tau phot	2.75	1	0 day	00:34:44	08:12:35	40
IQ Tau phot	2.75	1	0 day	00:38:36	08:21:08	40
Haro 6-13 phot	2.75	1	0 day	00:44:15	08:20:15	40
DL Tau phot	2.75	1	0 day	00:43:55	08:23:24	40
DM Tau phot	2.75	1	0 day	00:59:48	08:07:49	40
CI Tau phot	2.75	1	0 day	00:49:18	08:18:26	40
AA Tau phot	2.75	1	0 day	00:46:56	08:22:55	40
DN Tau phot	2.75	1	0 day	00:47:56	08:22:59	40
DO Tau phot	2.75	1	0 day	00:47:05	08:29:53	40

Name	Session time (hours)	Repeat	Separation	LST minimum	LST maximum	Elevation minimum
LkCa 15 phot	2.75	1	0 day	00:55:47	08:22:49	40
GO Tau phot	2.75	1	0 day	00:53:19	08:32:47	40
DR Tau phot	2.75	1	0 day	01:15:59	08:18:12	40
AB Aur phot	2.75	1	0 day	00:56:14	08:55:17	40
MWC 480 phot	2.75	1	0 day	01:00:30	08:57:03	40
GM Aur phot	2.75	1	0 day	00:55:59	08:54:23	40

Session Constraints:

Name	Scheduling constraints	Comments
CW Tau phot		For simplicity, we have included overheads by dividing the total estimated overhead equally among all observing bands into the Time/Session box.
RY Tau phot		For simplicity, we have included overheads by dividing the total estimated overhead equally among all observing bands into the Time/Session box.
FT Tau phot		For simplicity, we have included overheads by dividing the total estimated overhead equally among all observing bands into the Time/Session box.
IQ Tau phot		For simplicity, we have included overheads by dividing the total estimated overhead equally among all observing bands into the Time/Session box.
Haro 6-13 phot		For simplicity, we have included overheads by dividing the total estimated overhead equally among all observing bands into the Time/Session box.
DL Tau phot		For simplicity, we have included overheads by dividing the total estimated overhead equally among all observing bands into the Time/Session box.
DM Tau phot		For simplicity, we have included overheads by dividing the total estimated overhead equally among all observing bands into the Time/Session box.
CI Tau phot		For simplicity, we have included overheads by dividing the total estimated overhead equally among all observing bands into the Time/Session box.

Name	Scheduling constraints	Comments
AA Tau phot		For simplicity, we have included overheads by dividing the total estimated overhead equally among all observing bands into the Time/Session box.
DN Tau phot		For simplicity, we have included overheads by dividing the total estimated overhead equally among all observing bands into the Time/Session box.
DO Tau phot		For simplicity, we have included overheads by dividing the total estimated overhead equally among all observing bands into the Time/Session box.
LkCa 15 phot		For simplicity, we have included overheads by dividing the total estimated overhead equally among all observing bands into the Time/Session box.
GO Tau phot		For simplicity, we have included overheads by dividing the total estimated overhead equally among all observing bands into the Time/Session box.
DR Tau phot		For simplicity, we have included overheads by dividing the total estimated overhead equally among all observing bands into the Time/Session box.
AB Aur phot		For simplicity, we have included overheads by dividing the total estimated overhead equally among all observing bands into the Time/Session box.
MWC 480 phot		For simplicity, we have included overheads by dividing the total estimated overhead equally among all observing bands into the Time/Session box.
GM Aur phot		For simplicity, we have included overheads by dividing the total estimated overhead equally among all observing bands into the Time/Session box.

Session Source/Resource Pairs:

Session name	Source	Resource	Time
CW Tau phot	CWTau	C-phot	0.62 hour
CW Tau phot	CWTau	Ka-phot	0.34 hour

Session name	Source	Resource	Time
CW Tau phot	CWTau	Q-phot	0.32 hour
CW Tau phot	CWTau	X-phot	0.54 hour
CW Tau phot	CWTau	Ku-phot	0.46 hour
CW Tau phot	CWTau	K-phot	0.47 hour
RY Tau phot	RYTau	Ku-phot	0.46 hour
RY Tau phot	RYTau	X-phot	0.54 hour
RY Tau phot	RYTau	Ka-phot	0.34 hour
RY Tau phot	RYTau	C-phot	0.62 hour
RY Tau phot	RYTau	Q-phot	0.32 hour
RY Tau phot	RYTau	K-phot	0.47 hour
FT Tau phot	FTTau	X-phot	0.54 hour
FT Tau phot	FTTau	C-phot	0.62 hour
FT Tau phot	FTTau	Ka-phot	0.34 hour
FT Tau phot	FTTau	Q-phot	0.32 hour
FT Tau phot	FTTau	Ku-phot	0.46 hour
FT Tau phot	FTTau	K-phot	0.47 hour
IQ Tau phot	IQTau	Q-phot	0.32 hour
IQ Tau phot	IQTau	X-phot	0.54 hour
IQ Tau phot	IQTau	Ka-phot	0.34 hour
IQ Tau phot	IQTau	C-phot	0.62 hour
IQ Tau phot	IQTau	Ku-phot	0.46 hour
IQ Tau phot	IQTau	K-phot	0.47 hour
Haro 6-13 phot	Haro6-13	X-phot	0.54 hour
Haro 6-13 phot	Haro6-13	Q-phot	0.32 hour
Haro 6-13 phot	Haro6-13	Ku-phot	0.46 hour
Haro 6-13 phot	Haro6-13	C-phot	0.62 hour
Haro 6-13 phot	Haro6-13	Ka-phot	0.34 hour
Haro 6-13 phot	Haro6-13	K-phot	0.47 hour
DL Tau phot	DLTau	Ka-phot	0.34 hour
DL Tau phot	DLTau	Ku-phot	0.46 hour
DL Tau phot	DLTau	C-phot	0.62 hour
DL Tau phot	DLTau	Q-phot	0.32 hour
DL Tau phot	DLTau	X-phot	0.54 hour
DL Tau phot	DLTau	K-phot	0.47 hour
DM Tau phot	DMTau	Ku-phot	0.46 hour
DM Tau phot	DMTau	C-phot	0.62 hour
DM Tau phot	DMTau	Ka-phot	0.34 hour
DM Tau phot	DMTau	Q-phot	0.32 hour
DM Tau phot	DMTau	X-phot	0.54 hour
DM Tau phot	DMTau	K-phot	0.47 hour
CI Tau phot	CITau	Ku-phot	0.46 hour
CI Tau phot	CITau	Q-phot	0.32 hour
CI Tau phot	CITau	X-phot	0.54 hour

Session name	Source	Resource	Time
CI Tau phot	CITau	C-phot	0.62 hour
CI Tau phot	CITau	Ka-phot	0.34 hour
CI Tau phot	CITau	K-phot	0.47 hour
AA Tau phot	AATau	Ka-phot	0.34 hour
AA Tau phot	AATau	Q-phot	0.32 hour
AA Tau phot	AATau	C-phot	0.62 hour
AA Tau phot	AATau	Ku-phot	0.46 hour
AA Tau phot	AATau	X-phot	0.54 hour
AA Tau phot	AATau	K-phot	0.47 hour
DN Tau phot	DNTau	C-phot	0.62 hour
DN Tau phot	DNTau	X-phot	0.54 hour
DN Tau phot	DNTau	Ku-phot	0.46 hour
DN Tau phot	DNTau	Ka-phot	0.34 hour
DN Tau phot	DNTau	Q-phot	0.32 hour
DN Tau phot	DNTau	K-phot	0.47 hour
DO Tau phot	DOTau	Ku-phot	0.46 hour
DO Tau phot	DOTau	K-phot	0.47 hour
DO Tau phot	DOTau	Q-phot	0.32 hour
DO Tau phot	DOTau	Ka-phot	0.34 hour
DO Tau phot	DOTau	X-phot	0.54 hour
DO Tau phot	DOTau	C-phot	0.62 hour
LkCa 15 phot	LkCa15	Q-phot	0.32 hour
LkCa 15 phot	LkCa15	Ka-phot	0.34 hour
LkCa 15 phot	LkCa15	C-phot	0.62 hour
LkCa 15 phot	LkCa15	K-phot	0.47 hour
LkCa 15 phot	LkCa15	X-phot	0.54 hour
LkCa 15 phot	LkCa15	Ku-phot	0.46 hour
GO Tau phot	GOTau	X-phot	0.54 hour
GO Tau phot	GOTau	C-phot	0.62 hour
GO Tau phot	GOTau	Q-phot	0.32 hour
GO Tau phot	GOTau	K-phot	0.47 hour
GO Tau phot	GOTau	Ka-phot	0.34 hour
GO Tau phot	GOTau	Ku-phot	0.46 hour
DR Tau phot	DRTau	Ku-phot	0.46 hour
DR Tau phot	DRTau	K-phot	0.47 hour
DR Tau phot	DRTau	C-phot	0.62 hour
DR Tau phot	DRTau	Ka-phot	0.34 hour
DR Tau phot	DRTau	Q-phot	0.32 hour
DR Tau phot	DRTau	X-phot	0.54 hour
AB Aur phot	ABAur	Ka-phot	0.34 hour
AB Aur phot	ABAur	Q-phot	0.32 hour
AB Aur phot	ABAur	Ku-phot	0.46 hour
AB Aur phot	ABAur	K-phot	0.47 hour

Session name	Source	Resource	Time
AB Aur phot	ABAur	C-phot	0.62 hour
AB Aur phot	ABAur	X-phot	0.54 hour
MWC 480 phot	MWC480	Q-phot	0.32 hour
MWC 480 phot	MWC480	X-phot	0.54 hour
MWC 480 phot	MWC480	C-phot	0.62 hour
MWC 480 phot	MWC480	Ku-phot	0.46 hour
MWC 480 phot	MWC480	K-phot	0.47 hour
MWC 480 phot	MWC480	Ka-phot	0.34 hour
GM Aur phot	GMAur	Q-phot	0.32 hour
GM Aur phot	GMAur	Ka-phot	0.34 hour
GM Aur phot	GMAur	K-phot	0.47 hour
GM Aur phot	GMAur	Ku-phot	0.46 hour
GM Aur phot	GMAur	X-phot	0.54 hour
GM Aur phot	GMAur	C-phot	0.62 hour

Plan of dissertation: no

Technical Justification:

Combined telescopes:

No

Array configuration:

These are photometric explorations of the unresolved spectra of disks. The D configuration provides sufficiently coarse resolution at the high frequencies (Q, Ka) that the target emission will be unresolved. The sample targets do not have any known sources within a 30 arcsec radius, in an attempt to mitigate confusion in the low-resolution X/C-bands. Moreover, a search of archival C-band images (when available) and the S-band VLA Sky Survey images indicates that confusion with background sources within the X/C-band beams is not expected be problematic.

Subarrays:

N/A

Future semesters:

N/A

Scheduling restrictions:

The targets (at RA ~ 4-5 hours) are accessible at nighttime starting in August, rising late in the night during stable periods suitable for the high frequency measurements. Ideally they would be observed at night, although since image quality isn't the focus and the targets are bright enough for self-calibration, it may be suitable to observe into the morning if necessary. The desired elevation range is >40 degrees. There are no coordinated or fixed-date observations or other constraints in that sense.

LST Range Justification:

N/A

Receivers requested:

To cover the full broadband spectra of the targets and probe the continuum morphology from ~5-50 GHz, we are proposing to cycle through Q, Ka, K, Ku, X, and C bands with coarse (continuum) spectral resolution.

Samplers and correlator setup:

We will use the 3-bit samplers to maximize simultaneous continuum bandwidth. The standard continuum setup is sufficient for our purposes.

Mosaic requirements:

These are single-pointing observations: no mosaicking or OTF mapping are needed.

Sensitivity:

We targeted noise levels in each band based on (a) the expected flux densities of the targets extrapolated from higher frequencies, (b) the desire to sample the intra-band emission in post-processed ~1-2 GHz sub-bands, and (c) the desire to condense the observations in all the bands into as short a total time as possible, to mitigate concerns about variability. We can meet these aims for full-bandwidth (8, 6, or 4 GHz, depending on the band) RMS noise values of 48 uJy in Q, 19 uJy in Ka, 10 uJy in K, 6 uJy in Ku, 5.5 uJy in X, and 6 uJy in C. In assessing these target noise levels, we considered the effectively diminished bandwidths (10-15%) in Ku, X, and C bands from RFI and the variations in sensitivity expected across each band when splitting the full bandwidths into sub-bands (based on specific calculations with the ECT). Both of those effects are illustrated in the expected S/N = 5 limits marked in Figures 1 and 2 of the Scientific Justification, for clarity. The final images are expected to be sensitivity-limited.

Integration time:

The desired RMS values can be achieved in summer conditions with the targets at high (>50 degrees) elevation in on-source integration times of 2 min (Q), 3 min (Ka), 10 min (K), 10 min (Ku), 15 min (X), and 20 min (C): that is 60 minutes on-source per target. But the overheads are substantial. Based on previous experience and a detailed setup constructed in the OPT (SBID 40016228), we estimate that cycling through all the bands and performing the appropriate calibrations, pointing, and 3-bit sampler setups (etc.) necessary in each observing session will amount to ~105 minutes of overhead per target, which is considerably longer than implied by the ECT.

Dump time:

The default dump time of 3 s (5 s in C-band) is appropriate for this program. The default data rates for this setup are 15.8 MB/s (Q, Ka, K), 11.8 MB/s (Ku), 7.9 MB/s (X), and 4.7 MB/s (C). If we simplify by dividing the overheads evenly across all bands (as in the session setups), we estimate the raw data volume will be ~110 GB per target, or ~1.9 TB in total. If it is available, the online spectral binning factor should reduce that by a factor of 4, to ~470 GB.

Imaging considerations:

The only real issue for this program is associated with the wide fractional bandwidth. The goal is to split the data into 1-2 GHz sub-bands and image with standard CASA routines. If the full-bandwidth sensitivity in a single band is necessary (e.g., to estimate an upper limit), we will deploy the Taylor expansion imaging capabilities inside CASA for that purpose.

Polarimetric considerations:

N/A

RFI considerations:

RFI in the C, X, and Ku bands may affect ~10-15% of the bandpass, but standard flagging can excise the problematic data. This has been considered in estimates of the desired sensitivities (as noted in the RMS comments).

Joint considerations:

N/A

Other:

N/A

Array Configuration	D
Number of Antennas	25
Polarization Setup	Dual
Type of Image Weighting	Natural
Representative Frequency	44.0000 GHz
Receiver Band	Q
Approximate Beam Size	2.354"
Digital Samplers	3 bit
Elevation	High (50°-90°)
Average Weather	Summer
Calculation Type	Time
Time on Source	0h 2m 1s
Total Time	0h 3m 41s
Frequency Bandwidth	8.0000 GHz
Line Velocity Width	54,507.7196 km/s
RMS Noise (units/beam)	48.0000 µJy
RMS Brightness (temp)	0.0055 K
Confusion Level	0.0042 µJy

Samplers have been switched to 3-bit. The calculations now reflect the use of the 3-bit digital samplers. Compared to the 8-bit samplers there is about a 15% sensitivity penalty when using the 3-bit samplers.

Produced by the NRAO EVLA Exposure Calculator (Legacy version).

Array Configuration	D
Number of Antennas	25
Polarization Setup	Dual
Type of Image Weighting	Natural
Representative Frequency	10.0000 GHz
Receiver Band	X
Approximate Beam Size	10.356"
Digital Samplers	3 bit
Elevation	High (50°-90°)
Average Weather	Summer
Calculation Type	Time
Time on Source	0h 14m 36s
Total Time	0h 20m 22s
Frequency Bandwidth	4.0000 GHz
Line Velocity Width	119,916.9832 km/s
RMS Noise (units/beam)	5.5000 µJy
RMS Brightness (temp)	0.0006 K
Confusion Level	0.8967 µJy

Severe RFI effects. At this frequency band, part of the selected bandwidth may be severely affected by RFI. Visit the following web page for the RFI information at the VLA: https://science.nrao.edu/facilities/vla/docs/manuals/obsguide/modes/rfi Of the 8-12 GHz frequency span of the X-band, up to 15% could be affected by RFI. This should be properly accounted for while estimating the rms noise.

Produced by the NRAO EVLA Exposure Calculator (Legacy version).

Array Configuration	D
Number of Antennas	25
Polarization Setup	Dual
Type of Image Weighting	Natural
Representative Frequency	22.0000 GHz
Receiver Band	K
Approximate Beam Size	4.707"
Digital Samplers	3 bit
Elevation	High (50°-90°)
Average Weather	Summer
Calculation Type	Time
Time on Source	0h 10m 20s
Total Time	0h 17m 59s
Frequency Bandwidth	8.0000 GHz
Line Velocity Width	109,015.4393 km/s
RMS Noise (units/beam)	10.0000 µJy
RMS Brightness (temp)	0.0011 K
Confusion Level	0.0717 µJy

Samplers have been switched to 3-bit. The calculations now reflect the use of the 3-bit digital samplers. Compared to the 8-bit samplers there is about a 15% sensitivity penalty when using the 3-bit samplers.

Produced by the NRAO EVLA Exposure Calculator (Legacy version).

Array Configuration	D
Number of Antennas	25
Polarization Setup	Dual
Type of Image Weighting	Natural
Representative Frequency	33.0000 GHz
Receiver Band	Ka
Approximate Beam Size	3.138"
Digital Samplers	3 bit
Elevation	High (50°-90°)
Average Weather	Summer
Calculation Type	Time
Time on Source	0h 3m 8s
Total Time	0h 5m 27s
Frequency Bandwidth	8.0000 GHz
Line Velocity Width	72,676.9595 km/s
RMS Noise (units/beam)	19.0000 µJy
RMS Brightness (temp)	0.0022 K
Confusion Level	0.0167 µJy

Samplers have been switched to 3-bit. The calculations now reflect the use of the 3-bit digital samplers. Compared to the 8-bit samplers there is about a 15% sensitivity penalty when using the 3-bit samplers.

Produced by the NRAO EVLA Exposure Calculator (Legacy version).

Array Configuration	D
Number of Antennas	25
Polarization Setup	Dual
Type of Image Weighting	Natural
Representative Frequency	6.0000 GHz
Receiver Band	C
Approximate Beam Size	17.26"
Digital Samplers	3 bit
Elevation	High (50°-90°)
Average Weather	Summer
Calculation Type	Time
Time on Source	0h 19m 31s
Total Time	0h 27m 13s
Frequency Bandwidth	4.0000 GHz
Line Velocity Width	199,861.6387 km/s
RMS Noise (units/beam)	6.0000 µJy
RMS Brightness (temp)	0.0007 K
Confusion Level	4.1762 µJy

Severe RFI effects. At this frequency band, part of the selected bandwidth may be severely affected by RFI. Visit the following web page for the RFI information at the VLA: https://science.nrao.edu/facilities/vla/docs/manuals/obsguide/modes/rfi Of the 4-8 GHz frequency span of the C-band, up to 15% could be affected by RFI. This should be properly accounted for while estimating the rms noise.

Produced by the NRAO EVLA Exposure Calculator (Legacy version).

Array Configuration	D
Number of Antennas	25
Polarization Setup	Dual
Type of Image Weighting	Natural
Representative Frequency	15.0000 GHz
Receiver Band	Ku
Approximate Beam Size	6.904"
Digital Samplers	3 bit
Elevation	High (50°-90°)
Average Weather	Summer
Calculation Type	Time
Time on Source	0h 10m 3s
Total Time	0h 16m 35s
Frequency Bandwidth	6.0000 GHz
Line Velocity Width	119,916.9832 km/s
RMS Noise (units/beam)	6.0000 µJy
RMS Brightness (temp)	0.0007 K
Confusion Level	0.2640 µJy

Severe RFI effects. At this frequency band, part of the selected bandwidth may be severely affected by RFI. Visit the following web page for the RFI information at the VLA: https://science.nrao.edu/facilities/vla/docs/manuals/obsguide/modes/rfi Of the 12-18 GHz frequency span of the Ku-band, up to 12% could be affected by RFI. This should be properly accounted for while estimating the rms noise.

Produced by the NRAO EVLA Exposure Calculator (Legacy version).

Background and Motivation

In the classical "core accretion" model, the formation of a planetary system depends critically on the solid mass available in the progenitor circumstellar disk (Pollack et al. 1996) and the growth of those solids from μm-sized dust grains to $\sim$km-scale planetesimals (Birnstiel et al. 2016). Information about disk solids is accessed through the (sub)millimeter (100–500 GHz) to microwave (20–100 GHz) thermal continuum emitted by dust (Andrews 2020). If optical depths are low, the dust luminosity ($L_{\rm d}$) scales with mass (Beckwith et al. 1990), and the spectral index ($\alpha_{\rm d}$, where $S_\nu \propto \nu^{\alpha_{\rm d}}$) traces the grain size distribution (Draine 2006). Constraints on these fundamental aspects of planet formation come from statistical studies that track how $L_{\rm d}$ and $\alpha_{\rm d}$ evolve in populations of different ages (e.g., Barenfeld et al. 2016; Tazzari et al. 2021) as well as detailed examinations of the spatially resolved multifrequency continuum in individual disks (e.g., Pérez et al. 2012; Macías et al. 2021).

Most work has naturally focused on the high frequency (sub)millimeter bands, where the continuum is especially bright and easily measured with facilities like ALMA. However, those bands suffer (perhaps considerable) contamination from high optical depths (Andrews et al. 2018), especially from their inner regions and localized substructures (e.g., Ricci et al. 2012; Huang et al. 2018; Long et al. 2020). **Extending continuum measurements to lower frequencies – where the optical depths are lower – is essential** to learn more about the planet formation process. The high value ascribed to such data is reflected in the prominent roles they played in motivating future instruments (ALMA Band 1; Di Francesco et al. 2013) and observatories (ngVLA; Murphy et al. 2018). However, with sufficient data available for only a few special targets, we still know little about the microwave properties of dust disks ($L_{\rm d}$, $\alpha_{\rm d}$), the nature of contamination from additional emission mechanisms, or the behavior of the radio spectra from disk systems in general.

Objectives of Proposed Research

The key challenges to probing the dust disk properties in the microwave bands are to (a) sample a sufficiently broad spectral range to robustly measure $L_{\rm d}$ and the local $\alpha_{\rm d}$, and (b) quantify contamination from additional – potentially variable – emission mechanisms. We propose a pilot photometry study with the VLA in D configuration that deploys **contemporaneous** (within $\sim$1 hour) continuum measurements of disks with **dense and broad spectral coverage** at high sensitivity from $\sim$5–50 GHz to confront those challenges. This kind of detailed exploration of radio/microwave continuum spectra has not been systematically applied to disks before. A few famous cases stand out (e.g., HL Tau), but it is unclear if their properties are broadly applicable to other disks. Our goals are to:

> (1) Measure $L_{\rm d}$ and $\alpha_{\rm d}$ from the optically thin 20–50 GHz dust continuum emission, and compare with analogous estimates at >100 GHz; and
>
> (2) Characterize additional emission contributions from the radio spectrum extending to 5 GHz, while mitigating confusion from potential variability.

[**Goal 1**]

An optically thin dust continuum spectrum scales like $S_\nu \propto B_\nu(T)\kappa_\nu$, with $B_\nu(T)$ the Planck function at temperature T and κ_ν a grain absorption opacity (cross section per mass). The spectral shape of κ_ν is a diagnostic of grain sizes: flatter κ_ν implies a more top-heavy distribution of larger grains (Miyake & Nakagawa 1993). For the ISM, $\alpha_{\rm d} \approx 3.7$, corresponding to a steep κ_ν commensurate with μm-sized grains (Finkbeiner et al. 1999). But for disks, the average $\alpha_{\rm d} \approx 2.3$ at >100 GHz (Andrews 2020). This flatter spectrum is usually interpreted as evidence for grain growth (e.g., Beckwith & Sargent 1991; Ricci et al. 2010). However, resolved disk measurements signal that optically thick regions (with an effective $\alpha_{\rm d} \approx 2$) at these frequencies contaminate the $\alpha_{\rm d}$ estimates, mimicking the hallmarks of extensive growth (e.g., Tsukagoshi et al. 2016; Carrasco-González et al. 2016).

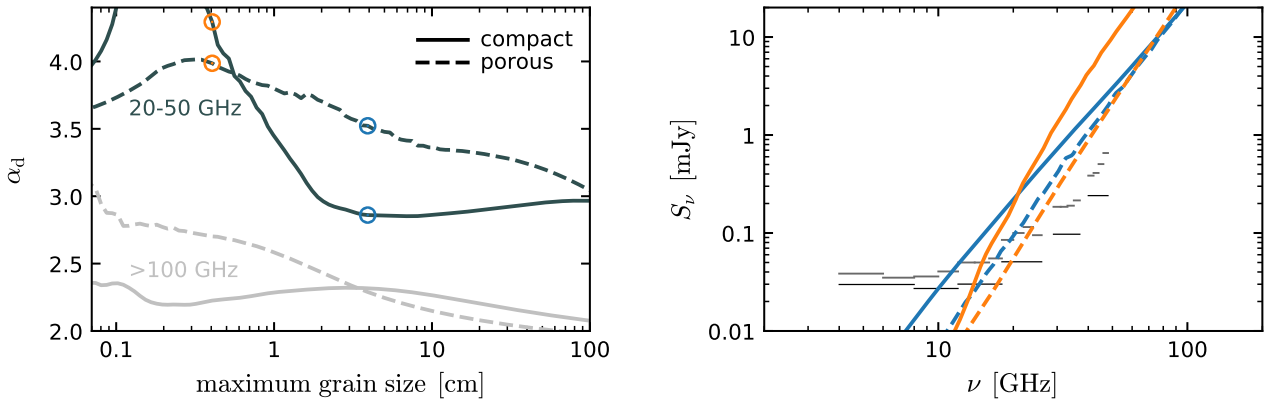

Figure 1: (*left*) Simulated spectral indices of the dust continuum (α_d) for compact (solid curve) and porous (50% filling fraction; dashed curve) dust with a power-law size distribution ($dn/da \propto a^{-3}$) as a function of the maximum grain size, in the microwave (20–50 GHz, as proposed here; dark curves) and (sub)millimeter (100–340 GHz; light curves). Calculations follow the approach of Sierra et al. (2019), using the opacity formulation of Birnstiel et al. (2018). (*right*) Simulated thermal dust continuum spectra for two examples of the maximum grain size (4 mm and 4 cm), for the compact (solid) and porous (dashed) cases. The gray (or black) horizontal segments mark the 5σ limits achieved by the proposed observations in 2 GHz (or full-band) chunks. All models were designed to be representative of the sample targets, and assume identical dust temperature and density profiles. At >100 GHz, these models have shallow spectra with $\alpha_d \approx 2.3$ because of high optical depths (where the index is primarily set by the behavior of the grain albedos; Liu 2019). We can better constrain the dust properties of disks by accessing their spectra at microwave frequencies.

We propose instead to measure α_d in a sample of bright disks based on their ∼20–50 GHz spectra. An illustration of the viability and benefits of this approach is provided in Figure 1. At these lower frequencies, the diminished κ_ν (by a factor >3–10) means only a minimal fraction of the dust emission can be contaminated by high optical depths. Moreover, the selected targets are bright enough to sample the in-band continuum in 1–2 GHz-wide bins across this important spectral range. That permits a characterization of the detailed shape of the optically thin dust continuum, where subtle deviations from a single power-law can be especially powerful diagnostics of the grain size distribution and secondary grain properties (e.g., porosity, composition; Wilner et al. 2005; Andrews et al. 2014). With an appropriate treatment of any additional emission sources (see below), such data will offer α_d measurements with uncertainties of only ∼0.3 (limited by the inter-band flux calibration accuracy), essentially the same quality as measurements at >100 GHz but with significantly improved ability to make helpful constraints on the important dust disk parameters.

[**Goal 2**]

The key complication to measuring L_d and α_d is the potential contribution of additional emission mechanisms, including bremsstrahlung from winds/outflows (Reynolds 1986; Pascucci et al. 2012), gyrosynchrotron radiation from active stellar coronae (Chiang et al. 1996), or electric dipole emission from spinning dust grains (Rafikov 2006; Hoang et al. 2018). These mechanisms produce different spectral shapes from the dust disk, as illustrated in Figure 2: bremsstrahlung has a flat to rising spectrum ($\alpha_{ff} \approx 0$ to 2); gyrosynchrotron is expected to have a falling spectrum ($\alpha_{gs} \approx -1$ to 0); and spinning dust should produce a marked deviation ("bump"). Moreover, bremsstrahlung (Ubach et al. 2017) and gyrosynchrotron (e.g., Phillips et al. 1991) radiation can vary in these systems on timescales as short as hours. To determine L_d and α_d, we need to disentangle the thermal dust spectrum from the 'contaminant' spectrum while accounting for that potential variability.

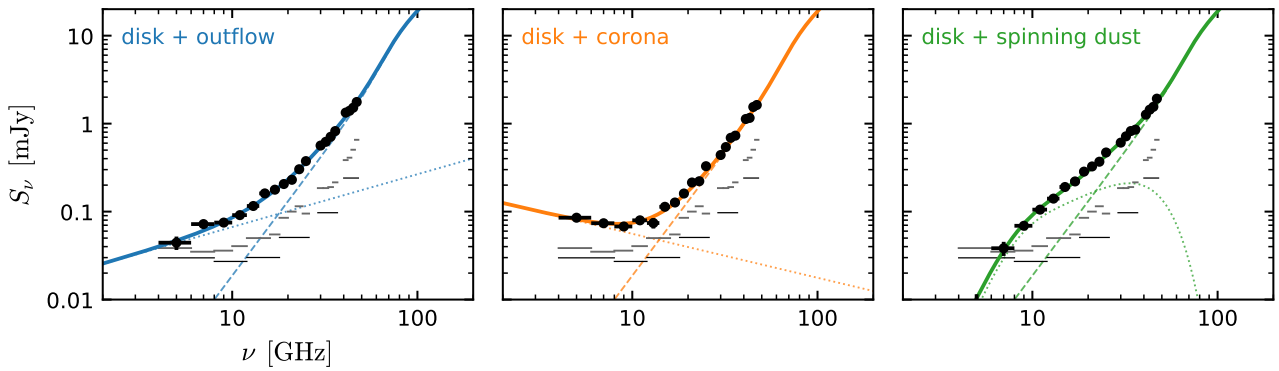

Figure 2: Simulated spectra for three representative scenarios. Each has the same (local) ν^3 thermal dust continuum, designed to be consistent with the sample mean spectrum at >100 GHz (dashed). From left to right, we have assumed there is an additional emission contribution dominated by (dotted) optically thick bremsstrahlung in an outflow, gyrosynchrotron radiation from an active stellar corona, or electric dipole emission from spinning small dust grains. The datapoints (black; with errorbars shown, but small) represent measurements in 2 GHz-wide sub-bands and are perturbed according to the expected noise and random inter-band offsets representative of flux calibration uncertainties up to 10%. The smooth curves represent the underlying models, which can be reproduced well by fitting the synthetic data with simple parameterizations. Annotations are as in Figure 1.

We aim to do this by densely sampling the spectra of disk targets in a near-contiguous swath from ∼5–50 GHz with contemporaneous measurements (in ∼1 hour). This broad coverage (particularly <20 GHz) and "high" spectral resolution (1–2 GHz) permits a clear characterization of 'contaminant' spectra, and the brevity of the observing window mitigates concerns around variability. While substantially improving our knowledge of fundamental dust disk properties, the proposed measurements will also inform us about these additional emission mechanisms themselves. Accessing the empirical behavior of this emission – e.g., luminosity, spectral morphology – is essential for linking accretion, outflows, and stellar activity in young stars (e.g., Purser et al. 2018; Pascucci et al. 2018).

Sample and Selection Criteria

We considered a sample from among the ∼150 disks in the nearby Taurus-Auriga complex. These targets have high elevations during stable, night-time hours in the 2022A D configuration schedule, making them well-suited for high frequency measurements. The primary selection criterion was a practical sensitivity cut. Viable targets include those that are predicted to have $S_Q \geq 1$ mJy based on a ν^3 extrapolation from 230 GHz (where measurements are available for effectively all Taurus disks). This is a conservative cut that likely under-estimates the true microwave emission levels, given the shallower spectra measured in most cases at >100 GHz. But we are focusing on the targets most likely to be bright to clearly demonstrate the potential of the methodology we're advocating without sensitivity-based caveats: we hope to expand the sample once we understand the issues and optimize the approach. After this flux cut, we discarded cases having another Taurus member (or a known background radio source) within 30″ to ensure that we avoid local confusion near the disk target at X/C-band, where the angular resolution is low (this removes multiple systems).

These criteria result in a sample of 17 targets, all of which are probably rather familiar to Taurus disk aficionados. Most of these targets have previous measurements of some sort in the VLA archive, but none at the depths, spectral coverage, and contemporaneity that we need to achieve the goals laid out above. Instead, those resources will be extraordinarily useful complements (see below).

Proposed Observations and Analysis

We propose to measure the Q, Ka, K, Ku, X, and C-band emission from the sample targets in the D configuration using the 3-bit samplers to maximize the simultaneous continuum bandwidth. Since the targets are bright, integration times are relatively short (from 2 minutes in Q-band to 20 minutes in C-band). The observations can proceed sequentially through the full spectral range in about an hour, limiting the potential for contamination by a time-variable emission contribution. For reasonable expectations (see Fig. 1 and 2), the predicted sensitivity is sufficiently high (S/N > 20) to consider the spectral behavior at finer resolution (1–2 GHz sub-bands). Initial analysis will focus on empirically modeling the spectra, with simple parameterizations that help disentangle the dust disk emission from additional mechanisms. We have verified that synthetic data are indeed capable of recovering the inputs with suitable precision to then compare the outcomes with more sophisticated dust model predictions (e.g., Fig. 1; see Andrews et al. 2014; Birnstiel et al. 2018).

We will also leverage these measurements against complementary constraints. Most importantly, this will involve joint analyses of the detailed spectra proposed here and archival high resolution imaging from ALMA and the VLA (available for nearly all of the proposed targets). The standard practice interprets such imaging data alone (Pérez et al. 2012, 2015; Tazzari et al. 2016; Carrasco-González et al. 2019), but that has some disadvantages. Aside from the considerable observational expense of high resolution imaging with sufficient sensitivity, quantifying the non-dust contamination for VLA images is often imprecise due to limited (contemporaneous) spectral coverage, and interpreting the resolved ALMA/VLA spectral index profile is complicated because of the disk regions where the ALMA emission is optically thick. Interpretations that fold in the densely-sampled (though spatially unresolved) broad spectrum coverage proposed here are expected to mitigate some underlying degeneracies and improve the inferences of key dust disk properties. Moreover, archival VLA data can also be used to better characterize the additional emission mechanisms in the microwave bands, particularly in terms of their long term (years to decades) variability.

Finally, the data from the proposed pilot program will broaden our still-limited perspectives on the microwave/radio spectra of disks, helping us design and coordinate future programs that can target a more diverse sample with the most efficiency. This latter point is especially crucial for facilitating a broader investigation of the dust properties in more expansive disk populations with the VLA, the upcoming low-frequency ALMA receiver sets (Bands 1 and 2), and ultimately the ngVLA.

References

Andrews et al. 2014, *ApJ*, 787, 148 • Andrews et al. 2018, *ApJ*, 865, 157 • Andrews 2020, *ARA&A*, 58, 483 • Barenfeld et al. 2016, *ApJ*, 827, 142 • Beckwith et al. 1990, *AJ*, 99, 924 • Beckwith & Sargent 1991, *ApJ*, 381, 250 • Birnstiel et al. 2016, *SSRev*, 205, 41 • Birnstiel et al. 2018, *ApJL*, 869, 45 • Carrasco-González et al. 2016, *ApJL*, 821, 16 • Carrasco-González et al. 2019, *ApJ*, 883, 71 • Chiang et al. 1996, *AJ*, 111, 355 • Di Francesco et al. 2013, arXiv:1310.1604 • Draine 2006, *ApJ*, 636, 1114 • Finkbeiner et al. 1999, *ApJ*, 524, 867 • Hoang et al. 2018, *ApJ*, 862, 116 • Huang et al. 2018, *ApJ*, 852, 122 • Liu 2019, *ApJL*, 877, 22 • Long et al. 2020, *ApJ*, 898, 36 • Macías et al. 2021, *A&A*, 648, 33 • Miyake & Nakagawa 1993, *Icarus*, 106, 20 • Murphy et al. 2018, *ASP Monograph*, 517 • Pascucci et al. 2012, *ApJL*, 751, 42 • Pascucci et al. 2018, *ASPC*, 517, 155 • Pérez et al. 2012, *ApJL*, 760, 17 • Pérez et al. 2015, *ApJ*, 813, 41 • Phillips et al. 1991, *ApJ*, 382, 261 • Pollack et al. 1996, *Icarus*, 124, 62 • Purser et al. 2018, *MNRAS*, 481, 5532 • Rafikov 2006, *ApJ*, 646, 288 • Reynolds 1986, *ApJ*, 304, 713 • Ricci et al. 2010, *A&A*, 512, 15 • Ricci et al. 2012, *A&A*, 540, 6 • Sierra et al. 2019, *ApJ*, 876, 7 • Tazzari et al. 2016, *A&A*, 588, 53 • Tazzari et al. 2021, *MNRAS*, in press • Tsukagoshi et al. 2016, *ApJL*, 829, 35 • Ubach et al. 2017, *MNRAS*, 466, 4083 • Wilner et al. 2005, *ApJL*, 626, 109